Communication

Effect of a Transverse Magnetic Field on Stray Grain Formation of Ni-Based Single Crystal Superalloy During Directional Solidification

WEIDONG XUAN, HUAN LIU, JIAN LAN, CHUANJUN LI, YUNBO ZHONG, XI LI, GUANGHUI CAO, and ZHONGMING REN

The effect of a transverse magnetic field on stray grain formation during directional solidification of superalloy was investigated. Experimental results indicated that the transverse magnetic field effectively suppressed the stray grain formation on the side the primary dendrite diverges from the mold wall. Moreover, the quenched experimental results indicated that the solid/liquid interface shape was obviously changed in a transverse magnetic field. The effect of a transverse magnetic field on stray grain formation was discussed.

DOI: 10.1007/s11663-016-0790-y

In recent years, owing to the excellent high temperature strength and creep durability, Ni-based superalloy single crystal turbine blades have been widely used in advanced aeroengines and industrial gas turbines. In industrial production, a single crystal turbine blade of Ni-based superalloy is usually obtained through a grain selector method, while an off-axial orientation dendrite may be formed because of the random nature of grain selector during directional solidification.[1–3] However, some work indicated that stray grains were easily formed on the edge of blade because of the primary dendrite with off-axial orientation in single crystal blades during directional solidification.[4–8] Due to the random orientation of stray grains, high-angle boundaries may be formed and decrease the mechanical properties. Therefore, many scientific research workers investigated the formation of stray grains during directional solidification,[4–25] and some methods of stray grain suppression are proposed, such as the optimization of cooling rate[26,27] and the application of spiral grain selector between the blade and the seed.[4,9] Unfortunately, stray grain formation is still a key defect that has not been effectively solved.

A transverse magnetic field has been extensively used to improve material microstructures and properties during solidification. Some reports show that a transverse magnetic field could influence many aspects of solidification,[28–30] such as the solid/liquid interface shape, the mushy zone length, the dendrite spacing, and the solute distribution. However, Liu *et al.*[6,7] and our previous work[8] indicate that the formation of stray grains on the side the primary dendrite diverges from the mold wall (*i.e.*, the diverging side) is derived from the enrichment of solute which leads to a large undercooling. According to these researches, utilizing a transverse magnetic field optimizes the microstructures and eliminates the stray grain defect of Ni-based single crystal superalloy.

Up to date, the effect of a transverse magnetic field on stray grain formation on the edge side for Ni-based single crystal superalloy during directional solidification has rarely been reported. The aim of this work is to investigate the effect of the transverse magnetic field on stray grain formation of superalloy PWA1483 during directional solidification. Experimental results indicated that the transverse magnetic field effectively suppressed the stray grain formation on the diverging side of sample.

The Ni-based single crystal superalloy PWA1483 was used in present work. The chemical compositions of PWA1483 are Cr 12.2, Co 9.0, Mo 1.9, W 3.8, Al 3.6, Ti 4.2, Ta 5.0, C 0.07 (wt pct), and Ni as balance. The single crystal seed with a diameter of 4 mm and length of 30 mm was cut from a single crystal rod with [001] crystal orientation in the solidification direction, and was placed at the bottom of crucible to control the grain number and the orientations of crystals.

The directional solidification apparatus under a transverse magnetic field is schematically shown in Figure 1(b). It mainly consisted of an electromagnet, a Bridgman-type furnace with a withdrawal system, and a temperature controller. The electromagnet could produce a static transverse magnetic field with a maximum intensity up to 1 T. The furnace temperature can reach to 1973 K (1700 °C) with a precision of ±1 K. The liquid Ga-In-Sn metal (LMC) pool with a water cooling jacket was used to cool the sample down. The temperature gradient in the sample was controlled through adjusting the temperature of the hot zone that was isolated from the LMC by a refractory baffle. The withdrawal velocity was controlled by a withdrawing device and could be continuously adjusted between 0.5 and 10000 μm/s.

In the experiments, the sample was heated to a certain temperature of 1773 K (1500 °C) and held for 5 minutes to ensure the seed was melted partly, and then was

WEIDONG XUAN, Materials Research Engineer, HUAN LIU, Ph.D. Student, JIAN LAN, Master, CHUANJUN LI, Associate Professor, and YUNBO ZHONG, XI LI, GUANGHUI CAO, and ZHONGMING REN, Professors, are with the State Key Laboratory of Advanced Special Steel & Shanghai Key Laboratory of Advanced Ferrometallurgy & School of Materials Science and Engineering, Shanghai University, Shanghai 200072, P.R. China. Contact e-mails: wdxuan@shu.edu.cn, zmren@shu.edu.cn

Manuscript submitted June 21, 2016.
Article published online August 22, 2016.

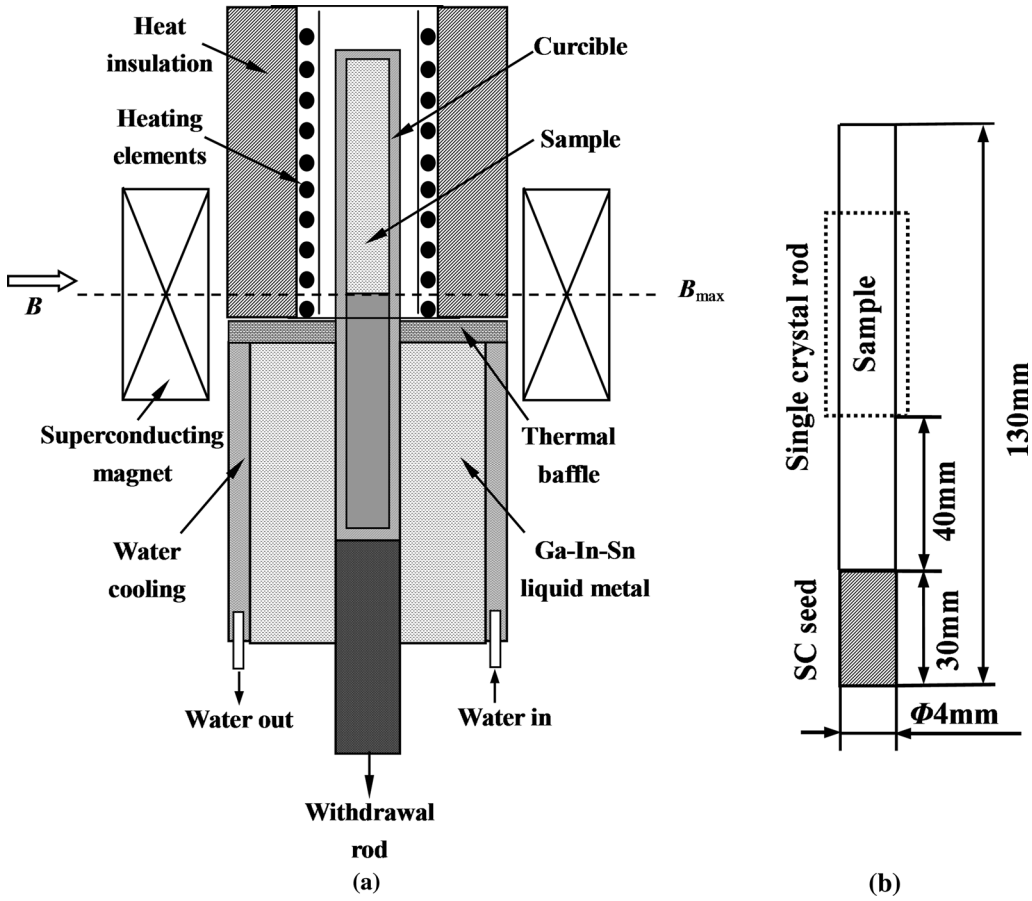

Fig. 1—Schematic diagram of experimental device: (*a*) schematic illustration of the Bridgman solidification apparatus; (*b*) sample and the position of the section planes in the sample.

directionally solidified in the Bridgman apparatus by withdrawing the crucible assembly downward at a constant withdrawal velocity. In this work, the temperature gradient was 50 K/cm, and the misorientation between the primary dendrite with <001> orientation and the solidification direction (*i.e.*, cylindrical direction) in the seed was about 28 deg. The longitudinal (paralleling to the solidification direction) microstructures of samples were observed in etched condition by Leica optical microscope (OM) to study the growth of dendrite and the formation of stray grain. The etchant solution was composed of $CuSO_4$ (4 g), HCl (20 ml), H_2SO_4 (12 ml), and H_2O (25 ml). The crystal orientations of primary dendrite and stray grains were investigated by electron backscatter diffraction (EBSD) technology.

Figure 2 shows the longitudinal microstructures of samples during directional solidification of the superalloy at a withdrawal velocity of 100 μm/s without and with a 0.7 T magnetic field. It was found that a stray grain was formed on the diverging side of sample without magnetic field (Figures 2(a) and (b)). However, when a transverse magnetic field was applied, no stray grain was observed and a single crystal was obtained in the entire sample, as shown in Figures 2(c) and (d). Therefore, it means that the transverse magnetic field suppresses the formation of stray grains in the present experimental conditions.

According to the stray grain formation theory,[4–25] the pinching-off dendrite fragments in the mushy zone and the heterogeneous nucleation in the front of liquid/solid interface are the main factors affecting stray grain formation. First, let us analyze the effect of pinching-off dendrite fragments in the mushy zone on stray grain formation during directional solidification. As we know, the pinching-off dendrite fragments transferred to the interface front induce the formation of stray grains due to the thermal–solutal convection.[10–12] Some research found that the thermal–solutal convection of alloy melt resulted from the coarse dendrite spacing and high element segregation which were usually formed at a low solidification velocity by Bridgman high rate solidification (HRS) during directional solidification,[10,11] whereas the pinching-off dendrite fragment was not formed at a high solidification velocity in the sample produced by liquid metal cooling technology (LMC) because of the sample's fine dendrite spacing and low element segregation.[31,32] Furthermore, stray grains arising from pinching-off dendrite fragment may appear at any location of the interface front.[33,34] Nevertheless, according to our previous researches[8,14,15] and present experimental results, stray grains always appear on the edge of sample, and the stray grain nucleation occurs in a more regular position compared with primary dendrite. Therefore, the detachment of the

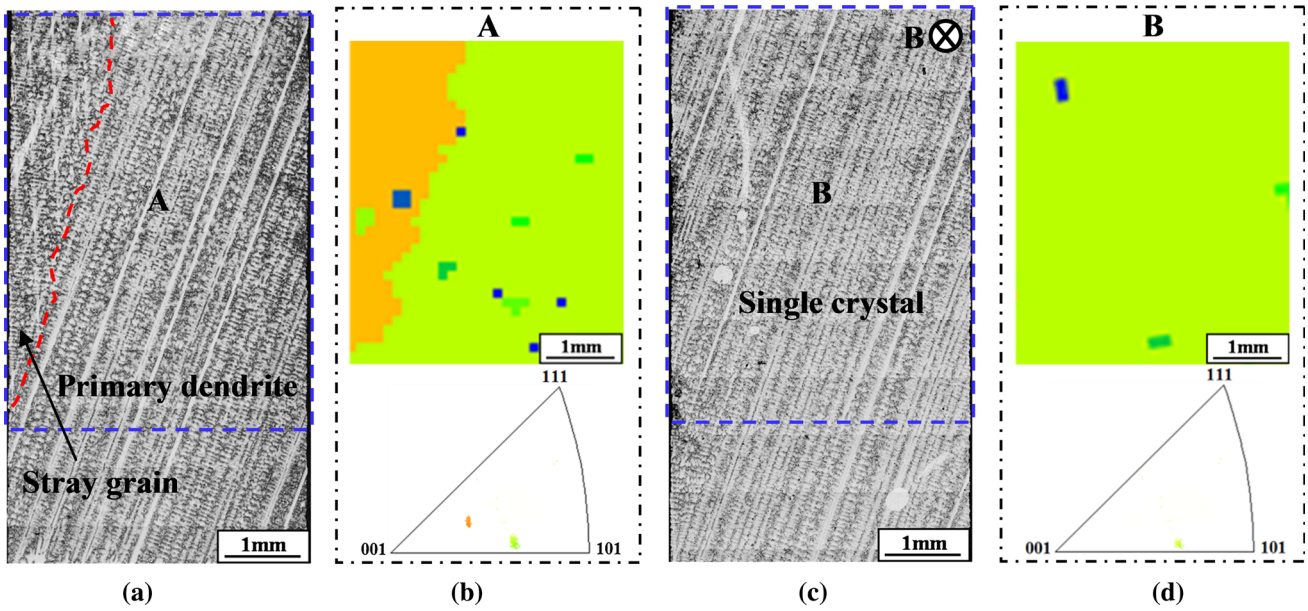

Fig. 2—(*a*) and (*c*) Longitudinal microstructures of directionally solidified sample for superalloy PWA1483 without and with a 0.7 T magnetic field ($v = 100$ μm/s), respectively; (*b*) and (*d*) corresponding EBSD orientation image maps and inverse pole figures of region A and B, respectively.

fragmented dendrite is not the main factor that results in the nucleation of stray grains on the edge of sample during directional solidification. Besides, numerous investigations indicate that the change of local solidification conditions, leading to a large undercooling and the heterogeneous nucleation on the edge of sample,[4–9] is a main factor that induces the formation of stray grains on the edge of sample. Based on the above analysis, the formation of stray grains on the edge of sample should be attributed to heterogeneous nucleation.

According to the classical nucleation theory, when the size of nucleus in liquid phase is larger than a certain critical value, a crystal is formed and expressed as activation energy ΔG^*.[35] According to a previous report from Kurz *et al.*,[36] the expression of nucleation activation energy and undercooling is as follows:

$$\Delta G^* \propto \Delta T^{-2}. \quad [1]$$

Equation [1] shows that the activation energy of nucleation is decreased with the increase of undercooling. However, present experimental results indicate that a stray grain only appears on the diverging side. It infers that the undercoolings on both sides are different for primary dendrite with a misorientation during directional solidification. As we know, during directional solidification, the undercooling ahead of dendrite tips mainly consists of thermal undercooling, solutal undercooling, curvature undercooling, and kinetic undercooling. The total undercooling ahead of dendrite tip, ΔT, can be written as follows:[37]

$$\Delta T = \Delta T_t + \Delta T_c + \Delta T_r + \Delta T_k, \quad [2]$$

where ΔT_t, ΔT_c, ΔT_r, and ΔT_k are thermal undercooling, solutal undercooling, curvature undercooling, and kinetic undercooling, respectively. According to a report from Rappaz *et al.*,[38] for most metallic alloys, the driving force of dendrite growth is mostly contributed by solutal undercooling and thermal undercooling, while curvature undercooling and kinetic undercooling are negligible during directional solidification. Our previous work[8] and some investigations[4–7] indicate that, for primary dendrite with a misorientation, the content of solute on the diverging side is higher than that on the converging side, the undercooling on the diverging side is also larger than that on the converging side. In addition, an investigation from Kurz *et al.*[39] indicates that the contribution of thermal undercooling is usually negligible compared with the solutal undercooling during directional solidification for primary dendrite with a steady-growth stage. Therefore, from Eq. [2], the undercooling ahead of dendrite tip, ΔT, mainly depends on the solutal undercooling, ΔT_c. In addition, according to the Eqs. [1] and [2], the relationship between the activation energy of nucleation and undercooling can be expressed as follows:

$$\Delta G^* \propto \Delta T_c^{-2}. \quad [3]$$

Equation [3] shows that the activation energy of nucleation decreases with the increase of undercooling. Therefore, this means that the formation of stray grains on the diverging side should be attributed to the heterogeneous nucleation derived from the solutal undercooling.

When a traverse magnetic field is employed to the directional solidification, two main effects of magnetic field on melt convection are formed. One is the electromagnetic braking (EMB) effect that is derived from the interaction between the moving conducting

Table I. Physical Parameters of the Ni-based Superalloy[46–49]

Physical Parameters	Magnitude
Electrical conductivity of solid (σ_S, Ω^{-1} m^{-1}) 1600 K (1327 °C)	0.75×10^6
Electrical conductivity of liquid (σ_L, Ω^{-1} m^{-1}) 1600 K (1327 °C)	0.67×10^6
Thermoelectric power of solid (S_S, μV K^{-1}) 1143 K (870 °C)	–10.95
Thermoelectric power of liquid (S_L, μV K^{-1}) 1773 K (1500 °C)	–16
Density of liquid alloy (ρ, Kg m^{-3}) 1613 K (1340 °C)	7.85×10^3

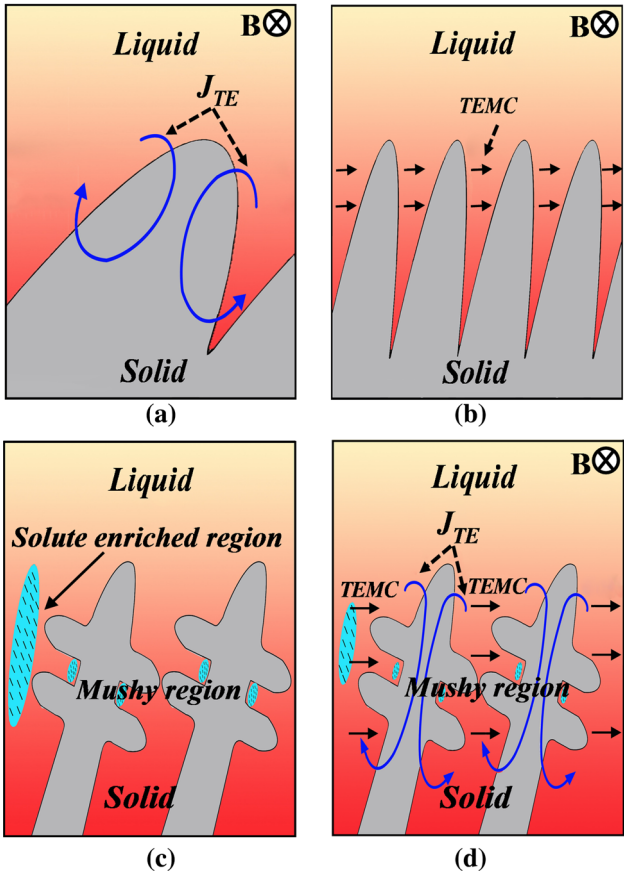

Fig. 3—(*a*) and (*b*) Schematic illustrations of the TE current and TEMC during directional solidification under a transverse magnetic field; (*c*) the distribution of the solute in the mushy region in the case of no magnetic field; (*d*) the effect of the TEMC on the distribution of the solute in the mushy region under a transverse magnetic field.

melt and the magnetic field, which suppresses the natural convection.[15,40,41] The other is the thermoelectric magnetohydrodynamic (TEMHD) effect that arises from the interaction between the thermoelectric current and the magnetic field, including the thermoelectric magnetic force (TEMF) in the solid phase and the thermoelectric magnetic convection (TEMC) in the liquid phase.[42–44]

The effect mechanisms of EMB and TEMC during directional solidification have been investigated theoretically and experimentally by some researches.[45] It is found that the fluid velocity increases as $B^{1/2}$ in weak magnetic field and then decreases as B^{-1} in high magnetic field. The maximum value of fluid velocity is obtained only when the TEMC is balanced with the viscous friction and EMB. The corresponding magnetic field intensity B_{max} can be written as follows:

$$B_{max} = \left(\frac{\rho(S_S - S_L)G}{l\sigma}\right)^{1/3}, \quad [4]$$

where ρ is the density of the alloy liquid; S_L, S_S are the thermoelectric powers of liquid and solid, respectively; l is the typical length scale and σ is the electrical conductivity. In order to easily understand the effect of magnetic field on melt convection, we evaluate the magnetic field intensity of maximum fluid velocity at the scale of dendrite (300 μm) based on Eq. [4]. The physical parameters of the Ni-based superalloy are listed in Table I. A magnetic field intensity of 1.22 T is obtained. This calculated result infers that the TEMC plays a key role during directional solidification when the magnetic field is smaller than 1.22 T. In addition, some studies indicate that the fluid velocity reaches a maximum value under an 1.2 T magnetic field.[15,44] Therefore, the transverse magnetic field induces the melt convection during directional solidification in present experimental conditions.

Besides, TEMF will affect dendrite and increase linearly with the increase of magnetic field since F_{TEMF} is directly proportional to B ($F_{TEMF} \propto B$).[45] An investigation indicates that the TEMF with a value of 10^5 N/m^3 is large enough to break down dendrites.[15,50] It is also found that the TEMF is larger than 10^5 N/m^3 when the magnetic field is higher than 3.8 T. This means that a 0.7 T high magnetic field will not result in the deformation, fracture, and deflection of dendrite, and a well-ordered dendrite structures is obtained in the entire sample during directional solidification. Likewise, the formation of stray grains on the diverging side during directional solidification under a transverse magnetic field should also be attributed to heterogeneous nucleation. Nevertheless, present experimental results demonstrated that no stray grain was formed on the edge of sample during seed melt-back under a 0.7 T magnetic field. It is inferred that the suppression of stray grains should be attributed to the change of undercooling on the edge of sample in a traverse magnetic field.

For the present experimental results of Ni-based superalloy, one possible explanation is that the TEMC will be generated during directional solidification under a traverse magnetic field, which gives rise to the movement of the solute along the direction of the TEMC, as shown in Figure 3. As a consequence, the content of solute element and the undercooling on the diverging side will decrease. In addition, according to

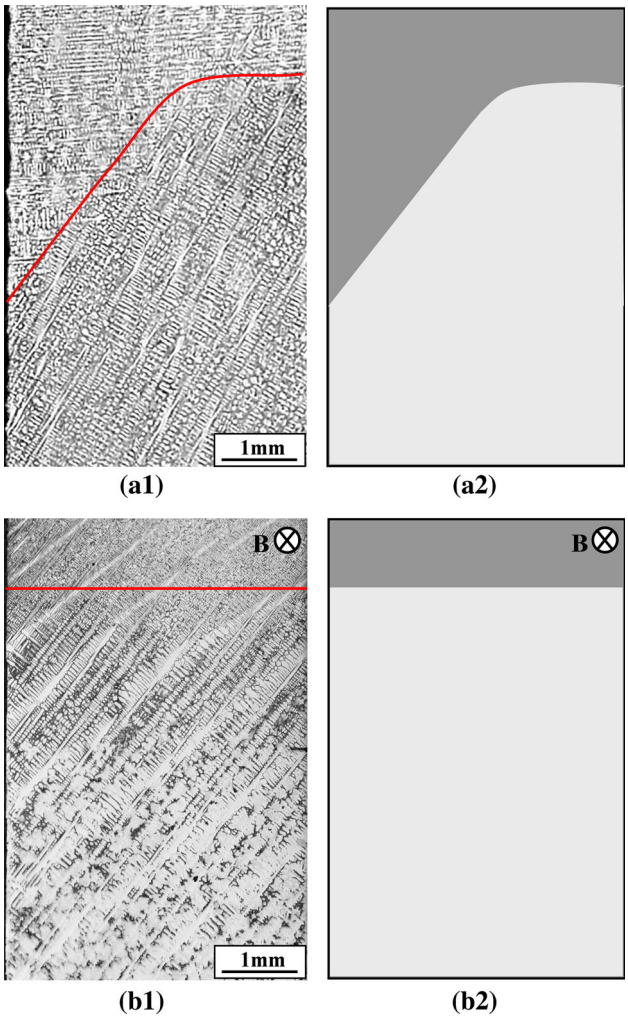

Fig. 4—(*a*) and (*b*) Morphologies of the quenched interface during directional solidification of superalloy at a withdrawal velocity of 50 μm/s without and with a 0.7 T magnetic field, respectively.

the interface stability theory, the convection and flow in the liquid near the interface obviously affect the growth behavior of dendrite. This means that TEMC will promote the growth of high-order dendrite on the diverging side and suppress the formation of stray grains during directional solidification.

In order to confirm the effect of TEMC on the primary dendrite growth behavior on the diverging side during solidification process, the quenching experiment was conducted. Figure 4 shows the quenched interface morphology at a withdrawal velocity of 50 μm/s without and with a 0.7 T magnetic field. It was found that in the case of no magnetic field, the solid/liquid interface shape was sloping from the diverging side to the converging side. However, the solid/liquid interface was nearly planar under a 0.7 T magnetic field. Therefore, it is implied that a traverse high magnetic field decreases the undercooling, promotes the growth of high-order dendrite, and further prevents the heterogeneous nucleation. As a consequence, the traverse magnetic field suppresses the formation of stray grains.

The effect of a transverse magnetic field on stray grain formation was investigated experimentally during the directional solidification of superalloy. Microstructures showed that the transverse magnetic field suppressed the formation of stray grains on the diverging side. In addition, the quenched experimental results indicated that the transverse magnetic field changed the solid–liquid interface shape. These results revealed that the TEMC formation under a transverse magnetic field should be responsible for the decrease of solute concentration and undercooling, and the suppression of stray grains on the diverging side.

This work was supported by the National Natural Science Foundation of China (Nos. U1560202, 51604172, 51401116), the Shanghai Municipal Science and Technology Commission Grant (Nos. 13521101102, 14521102900), and Shanghai Municipal Education Commission.

REFERENCES

1. H.J. Dai, H.B. Dong, N. D'Souza, J.C. Gebelin, and R.C. Reed: *Metall. Mater. Trans. A*, 2011, vol. 42A, pp. 3439–46.
2. S.F. Gao, L. Liu, N. Wang, X.B. Zhao, J. Zhang, and H.Z. Fu: *Metall. Mater. Trans. A*, 2012, vol. 43A, pp. 3767–75.
3. P. Carter, D.C. Cox, C.A. Gandin, and R.C. Reed: *Mater. Sci. Eng. A*, 2000, vol. 280, pp. 233–46.
4. N. D'Souza, P.A. Jennings, X.L. Yang, H.B. Dong, P.D. Lee, and M. McLean: *Metall. Mater. Trans. B*, 2005, vol. 36B, pp. 657–66.
5. Y.Z. Zhou: *Scripta Mater.*, 2011, vol. 65, pp. 281–84.
6. C.B. Yang, L. Liu, X.B. Zhao, J. Zhang, D.J. Sun, and H.Z. Fu: *Appl. Phys. A*, 2014, vol. 114, pp. 979–83.
7. X.B. Zhao, L. Liu, W.G. Zhang, M. Qu, J. Zhang, and H.Z. Fu: *Rare Met. Mater. Eng.*, 2011, vol. 40, pp. 0009–13.
8. W.D. Xuan, C.T. Li, H. Liu, C.J. Li, Z.M. Ren, Y.B. Zhong, X.F. Ren, K. Deng, X. Li, and G.H. Cao: *Metall. Mater. Trans. B* (Under Consideration).
9. N. Stanford, A. Djakovic, B.A. Shollock, M. McLean, and N. D'Souza: *Superalloys 2004*, K.A. Green, T.M. Pollock, H. Harada, T.E. Howson, R.C. Reed, J.J. Schirra, and S, Walston, eds., TMS, Warrendale, PA, 2004, pp. 719–26.
10. T.M. Pollock and W.H. Murphy: *Metall. Mater. Trans. A*, 1996, vol. 27, pp. 1081–94.
11. D.X. Ma and A. Bührig-Polaczck: *Metall. Mater. Trans. B*, 2009, vol. 40B, pp. 738–48.
12. X.L. Yang, P.D. Lee, and N. D'Souza: *JOM.*, 2005, vol. 3, pp. 40–44.
13. J.D. Miller and T.M. Pollock: *Acta Mater.*, 2014, vol. 78, pp. 23–36.
14. W.D. Xuan, Z.M. Ren, and C.J. Li: *Metall. Mater. Trans. A*, 2015, vol. 46A, pp. 1461–66.
15. W.D. Xuan, H. Liu, C.J. Li, Z.M. Ren, Y.B. Zhong, X. Li, and G.H. Cao: *Metall. Mater. Trans. B*, 2016, vol. 47B, pp. 828–33.
16. X.B. Meng, J.G. Li, S.Z. Zhu, H.Q Du, Z.H. Yuan, J.W. Wang, T. Jin, X.F. Sun, and Z.Q. Hu: *Metall. Mater. Trans. A*, 2014, vol. 45A, pp. 1230–37.
17. M. Meyer ter Vehn, D. Dedecke, U. Paul, and P.R. Sahm: *Superalloys 1996*, R.D. Kissinger, D.J. Deye, D.L. Anton, A.D. Cetel, M.V. Nathal, T.M. Pollock, and D.A. Woodford, eds., TMS, Warrendale, PA, 1996, pp. 471–79.
18. A.D. Bussac and C.A. Gandin: *Mater. Sci. Eng. A*, 1997, vol. 237, pp. 35–42.

19. M. Rappaz, C.A. Gandin, J.L. Desbiolles, and P. Thevoz: *Metall. Mater. Trans. A*, 1996, vol. 27A, pp. 695–705.
20. R.E. Napolitano and R.J. Schaefer: *J. Mater. Sci.*, 2000, vol. 35, pp. 1641–59.
21. T. Imwinkelried, J.L. Desbiolles, Ch-A. Gandin, M. Rappaz, S. Rossmann, and P. Thévoz: *Modeling of Casting, Welding and Advanced Solidification Processes VI*: *The Minerals, Metals&Materials Society*, 1993, pp. 63–70.
22. X.L. Yang, H.B. Dong, W. Wang, and P.D. Lee: *Mater. Sci. Eng. A*, 2004, vol. 386, pp. 129–39.
23. M. Rappaz, C.A. Gandin, J.L. Desbiolles, and P. Thevoz: *Metall. Mater. Trans. A*, 1996, vol. 27A, pp. 695–705.
24. N. D'Souza, M.G. Ardakani, M. McLean, and B.A. Shollock: *Metall. Mater. Trans. A*, 2000, vol. 31A, pp. 2877–86.
25. W.J. Boettinger, S.R. Coriell, A.L. Greer, A. Karma, W. Kruz, M. Rappaz, and R. Trivedi: *Acta Mater.*, 2000, vol. 46A, pp. 1461–66.
26. Q.Y. Xu, H. Zhang, X. Qi, and B.C. Liu: *Metall. Mater. Trans. B*, 2014, vol. 45B, pp. 555–61.
27. C. Ai, J. Zhou, H. Zhang, Y.L. Pei, S.S. Li, and S.K. Gong: *J. Alloys Compd.*, 2015, vol. 637, pp. 77–83.
28. X. Li, Y. Fautrelle, A. Gagnoud, D. Du, J. Wang, Z.M. Ren, H. Nguyen-Thi, and N. Mangelinck-Noel: *Acta Mater.*, 2014, vol. 64, pp. 367–81.
29. X. Li, D. Du, A. Gagnoud, Z.M. Ren, Y. Fautrelle, and R. Moreau: *Metall. Mater. Trans. A*, 2014, vol. 45A, pp. 5584–600.
30. J. Wang, Y. Fautrelle, H. Nguyen-Thi, Geinhart, H.L. Liao, X. Li, Y.B. Zhong, and Z.M. Ren: *Metall. Mater. Trans. A*, 2016, vol. 46A, pp. 1169–79.
31. L. Liu, T.W. Huang, J. Zhang, and H.Z. Fu: *Mater. Lett.*, 2007, vol. 61, pp. 227–230.
32. A.J. Elliott, S. Tin, W.T. King, S.C. Huang, M.F.X. Gigliotti, and T.M. Pollock: *Metall. Mater. Trans. A*, 2004, vol. 35, pp. 3221–31.
33. H. Yasuda, I. Ohnaka, K. Kawasaki, A. Sugiyama, T. Ohmichi, J. Iwane, and K. Umetani: *J. Cryst. Growth*, 2004, vol. 262, pp. 645–52.
34. R.H. Mathiesen and L. Arnberg: *Mater. Sci. Eng. A*, 2005, vols. 413–414, pp. 283–87.
35. D.A. Porter and K.E. Easterling: *Phase Transformations in Metals and Alloys*, 2nd ed., Chapman & Hall, London, 1992, p. 193.
36. M. Gäumann, R. Trivedi, and T.V. Kurz: *Mater. Sci. Eng. A*, 1997, vols. 226–228, pp. 763–69.
37. J. Lipton, M. Glicksman, and W. Kurz: *Metall. Trans. A*, 1987, vol. 18, pp. 341–45.
38. M. Rappaz and Ch.-A. Gandin: *Acta. Metall. Mater.*, 1993, vol. 41, pp. 345–60.
39. J. Lipton, M.E. Glicksman, and W. Kurz: *Mater. Sci. Eng.*, 1984, vol. 65, pp. 57–63.
40. C. Vives and C. Perry: *Int. J. Heat Mass Transf.*, 1987, vol. 30, pp. 479–96.
41. W.E. Langlois and K.J. Lee: *J. Cryst. Growth*, 1983, vol. 62, pp. 481–86.
42. W.J. Boettinger, F.S. Biancaniello, and S.R. Coriell: *Metall. Mater. Trans. A*, 1981, vol. 12A, pp. 321–27.
43. P. Lehmann, R. Moreau, D. Camel, and R. Bolcato: *Acta Mater.*, 1998, vol. 46, pp. 4067–79.
44. W.D. Xuan, Z.M. Ren, and C.J. Li: *J. Alloys Compd.*, 2015, vol. 621, pp. 10–17.
45. X. Li, Y. Fautrelle, and Z.M. Ren: *Acta Mater.*, 2007, vol. 55, pp. 3803–13.
46. Y.Y. Khine and S. Walker: *J. Cryst. Growth*, 1998, vol. 183, pp. 150–58.
47. P. Dolda, F.R. Szofranb, and K.W. Benz: *J. Cryst. Growth*, 2006, vol. 291, pp. 1–7.
48. H. Yasuda, T. Yoshimoto, T. Mizuguchi, Y. Tamura, T. Nagira, and M. Yoshiya: *ISIJ Int.*, 2007, vol. 47, pp. 612–18.
49. G. Pottlacher, H. Hosaeus, B. Wilthan, E. Kaschnitb, and A. Seifter: *Thermochim. Acta*, 2002, vol. 382, pp. 255–67.
50. X. Li, Y. Fautrelle, K. Zaidat, A. Gagnoud, Z.M. Ren, R. Moreau, Y.D. Zhang, and C. Esling: *J. Cryst. Growth*, 2010, vol. 312, pp. 267–72.